

Effect of Hand Dynamics on Virtual Fixtures for Compliant Human-Machine Interfaces*

Panadda Marayong^{1†}

Gregory D. Hager^{2‡}

Allison M. Okamura^{1§}

¹Department of Mechanical Engineering, ²Department of Computer Science
Engineering Research Center for Computer-Integrated Surgical Systems and Technology
The Johns Hopkins University
Baltimore, MD 21218, USA

ABSTRACT

In human-machine interfaces with joint/link compliance, human hand dynamics can have a detrimental effect on system performance. This paper investigates the effect of human dynamics on the effectiveness of a virtual fixture implemented on an admittance-controlled robot with joint compliance. Two open-loop control methods are proposed for creating a virtual fixture that prevents the user from entering a forbidden region: one that compensates for hand dynamics, and one that predicts overshoot based on the user's current velocity. The methods determine a "safe" location of the virtual fixture that prevents the user from entering the true forbidden region. A first experiment was conducted to determine hand dynamic parameters (mass, damping, and stiffness) and evaluate their relationship to the force applied by the user on the interface. A second experiment demonstrated that both methods for creating safe virtual fixtures prevent the user from entering the forbidden region, even when the interface has significant joint compliance.

CR Categories: H.5.2 [Information Interfaces and Presentation]: User Interfaces—Evaluation/methodology; H.5.2 [Information Interfaces and Presentation]: User Interfaces—User-centered Design; I.2.9 [Artificial Intelligence]: Robotics—Kinematics and Dynamics; I.2.9 [Artificial Intelligence]: Robotics—Operator Interfaces

Keywords: hand dynamics, virtual fixtures, compliant human-machine interfaces, admittance control

1 INTRODUCTION

The goal of human-machine cooperative systems is to enhance user performance in tasks at the limits of human physical abilities. Cooperative systems combine the precision and the repeatability of a robot with the intelligence and experience of a human operator. Virtual fixtures are added to a cooperative system to guide the end-effector along desired paths in the workspace (guidance virtual fixtures) or to prevent the end-effector from entering undesired regions (forbidden-region virtual fixtures). Virtual fixtures can be implemented on both impedance-controlled systems [1, 18, 19] and admittance-controlled systems [4, 17, 14]. In this work, we are primarily interested in the implementation of forbidden-region virtual fixtures in an admittance-controlled cooperative robot with joint compliance.

*This material is based upon work supported by the National Science Foundation under Grant No. ITR-0205318.

[†]e-mail: pmarayong@jhu.edu

[‡]e-mail: hager@cs.jhu.edu

[§]e-mail: aokamura@jhu.edu

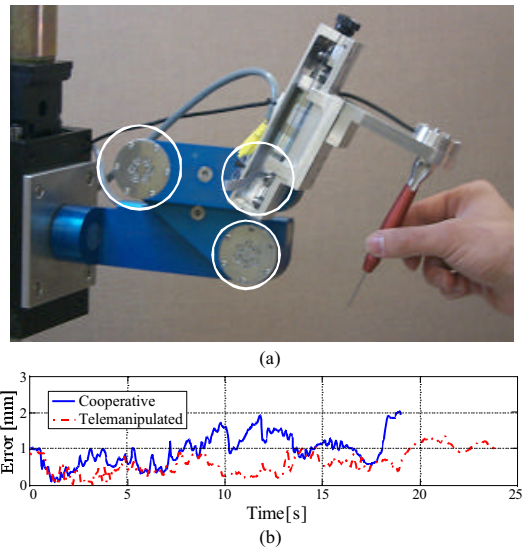


Figure 1: (a) The Steady Hand Robot is an example of an admittance-controlled cooperative manipulator. Locations of joint compliance are circled. (b) Comparison of the tool positioning error when the robot is cooperatively manipulated versus telemanipulated.

In cooperative manipulation systems, the user and the robot simultaneously grasp the end-effector/tool. Figure 1a shows the JHU Steady-Hand Robot (SHR) [20], a seven-degree-of-freedom cooperative manipulator. Admittance-controlled robots operate by moving at a velocity proportional to the force applied. Hence, in admittance-controlled cooperative manipulators, the human user applies a disturbance force to the robot in order to achieve motion. Despite the high rigidity and non-backdrivability of an admittance-controlled system, we have discovered in previous experiments that even small joint and link compliance visibly degrade virtual fixture performance, since the virtual fixture location becomes incorrectly defined when there are unmodeled deviations in the mapping from robot joint space to the environment/task space. This is especially problematic in tasks such as microsurgery, where precision at the micron-level is required [24].

Virtual fixture location errors are amplified because the human user constantly applies a disturbance to the system. Figure 1b illustrates tool position errors observed with an external optical tracking system on the SHR [13]. When the user is operating the robot in a cooperative mode, the errors are higher than when the same robot is telemanipulated. In addition to the deflection of the robot due to voluntary motion, the inherent mechanical parameters of the human hand also generate dynamics that result in undesired involuntary motion. Thus, link or joint compliance and human hand dynamics should be considered in order to achieve accurate virtual fixtures in admittance-controlled cooperative manipulators.

It is recognized that link and joint compliance presents significant challenges in controlling robotic systems. Much of the previous work on modelling and control of flexible manipulators has focused on large and long manipulators carrying heavy loads for applications such as hazardous waste management and space applications [7, 15, 23]. In minimally invasive surgical robots, Beasley et al. [3] developed a method to measure the kinematic error due to port displacement and instrument shaft flexion. The work implemented a model-based method in controlling the end-effector position, without consideration of human dynamics. Other work considering human dynamics in human-machine cooperative systems mainly focuses on force control applications for impedance-controlled systems [10, 11].

To investigate virtual fixture performance with hand dynamics, a 1-DOF admittance-controlled testbed was used. A spring element was added to simulate joint compliance. Two open-loop controllers were proposed to define a virtual fixture position that prevents the user from entering the true forbidden region. The virtual fixture can be viewed as a safety margin whereby its distance to the true forbidden region can vary depending on the dynamics of the system. We named this the *dynamic virtual wall*. The rest of the paper begins with the details of the two proposed controller methods used to define the dynamic virtual wall including the Velocity-Based method and the Hand-Dynamic method. The first method predicts the overshoot into the forbidden region based on the instantaneous tool position and velocity to calculate the virtual wall distance. In the Hand-Dynamic method, the hand dynamics during its involuntary motion is used to determine the virtual wall position. With this method, the effective human hand dynamic parameters (mass, damping and stiffness coefficients) are needed. Section 3 describes the model and the experiment used to identify these parameters. In Section 4, the two methods were implemented and compared experimentally.

2 DYNAMIC VIRTUAL WALLS

The goal of forbidden-region virtual fixtures is to prevent the end-effector (both position and orientation) from entering into an undesired region. For a 1-DOF system, this reduces to simply preventing the tool tip from passing a fixed limit. In a system with joint compliance, the tool position error due to the compliance can be corrected by moving the actuated joint. In conventional forbidden-region virtual fixtures, this can be accomplished with a PID controller on the tool position. As a result, the controller is effective only when there is an error in the system, implying that some amount of penetration into the undesired region has already occurred. In addition, the human operator may not respond immediately to the virtual fixture contact, so human hand dynamics can contribute to involuntary motion into the forbidden region.

A straightforward solution to this problem is to place the virtual fixture such that there is a safety margin between it and the true forbidden region. The question raised in this paper is how large this safety margin should be. We propose the creation of a movable virtual fixture, which we call the *dynamic virtual wall*, whose distance from the true forbidden region depends on the instantaneous system dynamics. The distance between the boundary of the forbidden region and the dynamic virtual wall should equal the amount of potential overshoot due to human hand dynamics and robot joint compliance. For the remainder of the paper, let x_t denote the tool position at the current time step, x_f denotes the boundary of the true forbidden region, and $x_w = x_f + d$ denote the dynamic virtual wall position for a desired safety margin d .

In this section, we provide two methods for choosing d to ensure that $x_t < x_f$, despite the effects of robot and hand dynamics. Both methods rely on the prediction of future tool positions based on information about the system dynamics at the current time step. We

currently consider implementation on a 1-DOF system, however, the methods can be extended to include more degrees of freedom. We assume the hand maintains contact with the tool at all times, so the positions of the hand and the tool are the same.

2.1 Velocity-Based Method

The Velocity-Based Method provides an ad hoc solution to determine the amount of overshoot that may occur if the operator continues moving with the current instantaneous velocity. The future tool position is predicted from the current tool position and velocity. The condition applied by the method to determine the dynamic virtual wall position, x_w , is

$$x_w = \begin{cases} x_t & \text{if } x_t + \Delta t v_t > x_f \\ x_f & \text{otherwise} \end{cases}, \quad (1)$$

where x_t and v_t are the position and velocity of the tool at the current time step, respectively, and Δt is the time step used to calculate a future tool position. In our implementation, $\Delta t = 120\text{msec}$, since this represents the time required for a human to voluntarily respond to a tactile stimulus [6]. During this time, the applied force can be assumed to be constant. The tool position, x_t , is calculated from the joint stiffness coefficient and the human-applied force using Hooke's law. Hence, the Velocity-Based Method includes the influence of human inputs and the joint compliance of the robot.

2.2 Hand-Dynamic Method

Studies performed by Bizzi et al. [5] provided strong evidence that the nervous system uses an equilibrium-point control to guide joint movements. The muscle force used to maintain a limb posture determines the equilibrium position of the limb and the stiffness in the joints. Limb trajectories result from joint torques commanded by the nervous system to follow a series of equilibrium postures. The requisite force exerted by the limb is proportional to the limb stiffness and the instantaneous difference between the virtual equilibrium position and the actual limb position:

$$f_{\text{exerted}} = k_h(x_{\text{virtual}} - x_{\text{actual}}). \quad (2)$$

The hypothesis greatly simplifies the analysis of the mechanical interactions between human motion and a complex dynamic environment.

Due to joint compliance on an admittance-controlled robot, the hand and the tool can continue moving despite the presence of a virtual fixture. Our analysis applies the equilibrium-point control model to capture the instantaneous involuntary hand motion upon contact with the virtual fixture. It enables us to predict the amount of overshoot past a virtual fixture due to the dynamics of the human hand about the equilibrium point. This overshoot is then used to determine the position of the dynamic virtual wall.

In a human-machine cooperative system with an admittance-controlled robot, the operator actively exerts forces on a tool, and the robot moves with a (typically slow) speed proportional to the force applied. In applications such as microsurgery, the range of hand motion during tool manipulation is limited. Most of the motion occurs from the hand and the wrist, while the forearm and the upper arm remain stationary. For the application of cooperative robots in microsurgery, it is realistic to assume that only the human's hand and wrist dynamics need to be considered in our equilibrium-point control model.

The hand is modeled with a mass-spring-damper model. Prior work has shown that upper-extremity human joints are accurately modeled with a linear second order system [8, 21, 9, 12, 22]. Figure 2 represents the interaction between the hand and the robot at the virtual wall. Since the hand is assumed to maintain contact with

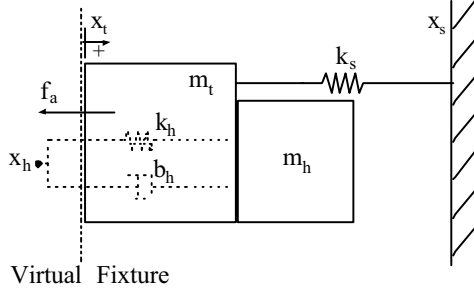


Figure 2: Hand and system model at the virtual wall where x_s and x_t denote the position of the stage and the tool and hand, respectively. m_t is the tool mass. m_h , b_h and k_h are the hand dynamic parameters. x_h is the hand virtual equilibrium-position. k_s is the joint stiffness coefficient. f_a is the force applied by the user.

the tool at all times, the tool and hand are at the same position, x_t . A force sensor is placed between the tool and stage. Conservation of energy of the system shown in Figure 2 is used to determine the amount of overshoot as described in the remainder of this section.

The energy immediately before and after virtual fixture contact must balance as

$$KE_1 + PE_1 = KE_2 + PE_2, \quad (3)$$

where KE and PE are the kinetic and the potential energy term, respectively. The subscripts 1 and 2 denote the response immediately before and after passing the virtual fixture, respectively. The kinetic energy is the result of the motion of the tool and the hand (m_t and m_h). The potential energy results from the energy stored in the springs with stiffness coefficients k_h and k_t . Dissipation of energy due to damping is neglected to give an upper bound on overshoot. Immediately before the tool passes the virtual fixture, the position of the tool is at x_{t1} . The maximum tool position after passing the virtual fixture (x_{t2}) occurs when its velocity becomes zero. Hence, KE_2 is zero. Thus, the conservation of energy can be expressed as

$$\begin{aligned} \frac{1}{2}(m_t + m_h)\dot{x}_{t1}^2 + \frac{1}{2}k_s(x_{t1} - x_s)^2 + \frac{1}{2}k_h(x_h - x_{t1})^2 \\ = \frac{1}{2}k_s(x_{t2} - x_s)^2 + \frac{1}{2}k_h(x_h - x_{t2})^2 \end{aligned} \quad (4)$$

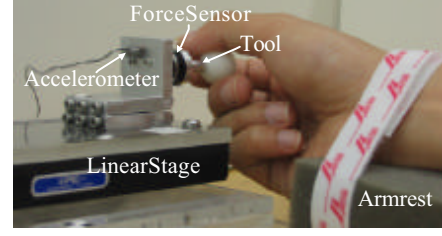
where x_s is the stage position and $x_h = \frac{f_a}{k_h} + x_{t1}$, based on the equilibrium-point control assumption (Equation 2) and $(x_{t1} - x_s) = \frac{f_a}{k_s}$ from Hooke's law. If the dynamic wall is placed at x_{t1} , the stage stops moving and the stage position (x_s) remains constant. The maximum hand position (x_{t2}) can then be calculated by solving a quadratic equation of the form

$$x_{t2} = \frac{-b \pm \sqrt{b^2 - 4ac}}{2a}, \quad (5)$$

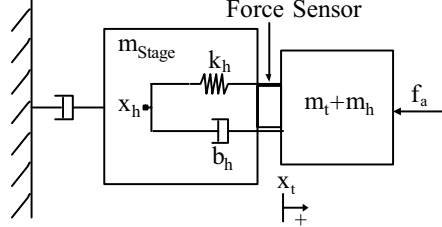
$$\begin{aligned} \text{where } a &= k_s + k_h \\ b &= -2(f_a + k_h x_{t1} + k_s x_s) \\ c &= k_s x_s^2 + (2f_a + k_h x_{t1})x_{t1} \\ &\quad - \frac{f_a^2}{k_s} - (m_t + m_h)\dot{x}_{t1}^2 \end{aligned}$$

The algorithm then computes the position of the dynamic virtual wall using:

$$x_w = \begin{cases} x_{t1} & \text{if } x_{t2} > x_f \\ x_f & \text{otherwise} \end{cases} \quad (6)$$



(a)



(b)

Figure 3: (a) Experimental setup for hand dynamic parameter estimation. (b) The linear second-order system model used in determining hand parameters.

3 IDENTIFICATION OF THE MECHANICAL IMPEDANCE OF HUMAN HAND

In order to implement the Hand-Dynamic Method, the effective mass and stiffness of the hand in an active pushing task are needed. Previous studies suggest that the dynamic parameters of an active finger change when different forces are exerted [8]. Previous experiments with grasping of a stylus [12] and a haptic knob [9] indicate that hand/wrist mass, stiffness, and damping increase as grip force increases. In order to accurately capture the dynamics of tool manipulation in an active pushing task, both applied force and the gripping force need to be considered simultaneously. Other previous work on the identification of a human hand or finger dynamic parameters include [21, 22]. However, to the best of the authors' knowledge, this work presents the first attempt to identify the mechanical impedance of the hand, considering both the applied and gripping forces.

3.1 Experimental Apparatus and Procedure

The apparatus used to determine the hand dynamic parameters is a 1-DOF cooperative robot with no joint compliance. The system includes a low-friction linear stage, an accelerometer, an optical encoder, a force sensor, and a tool rigidly attached to both the force sensor and the linear stage (Figure 3a). A spherical Delrin knob was used as the tool handle. A highly backdrivable motor (1:1 gear ratio) was used to drive the stage. A constraint with soft padding was used to minimize arm motion and keep the forearm parallel to the horizontal plane. Only the user's hand and wrist were allowed to move.

The users were instructed to hold the tool with three different grip force levels, corresponding to a normal, soft, and hard grip of the tool. The grip force was not explicitly measured. For each grip force level, the users were asked to push the stage at four different target forces (2, 4, 6, and 8 N), presented in random order. To push the stage, the user grasped the tool and exerted a translational force. Before the target translational force was reached, the stage remained stationary using PD control, and the amount of the applied force with respect to the target force was displayed on a monitor. Once the applied force was reached and maintained



Figure 4: Setup for the experiment to determine hand dynamic parameters.

within 12% of the target force (slightly higher than the 10% JND [2]) for three seconds, the display was turned off and the stage was allowed to move freely. This creates a negative impulse on the hand. The computer then recorded the acceleration and the position of the stage. The stage velocity was computed offline from the recorded position. Since the hand is assumed to maintain contact with the tool (rigidly attached to the stage) at all times, the stage position and acceleration measured are the same for the hand. Milner and Franklin [16] reported that muscle stretch reflex responses can be observed as fast as within 20-30msec. Thus, the data to identify the hand parameters was collected within 20msec of the start of stage motion. The data were collected every 1msec.

Eight right-handed users, including four females and four males between the ages of 23 and 35 participated in the experiment. Each user sat in front of a computer monitor and the apparatus, with his/her hand and the apparatus hidden from view (Figure 4). The users could grasp the tool whichever way they felt comfortable and were asked to keep the grasping method constant throughout the experiment. This usually resulted in a two- or three-fingered grasp. The users performed three trials for each target force. The users completed the trials with the normal grip force before performing the trials with soft and hard grip force. This results in a total of 36 trials per user. Practice time was given prior to the actual experiment. The users were allowed some rest time between trials to minimize hand fatigue.

3.2 Hand Model and Fitting Technique

Figure 3b represents the system model used in estimating hand dynamic parameters. With the equilibrium-point control assumption [5], the force balance equation with parameters m , b , and k , representing the mass, damping, and stiffness coefficients of the hand, can be expressed as follows:

$$(m_t + m_h)\ddot{x}(t) = b_h(\dot{x}_h - \dot{x}(t)) + k_h(x_h - x(t)) - f_a(t), \quad (7)$$

where the x , \dot{x} , and \ddot{x} denote the position, velocity, and acceleration of the hand (and tool/stage), respectively. x_h and \dot{x}_h are the position and velocity of the hand equilibrium point, respectively. f_a is the human-applied force measured by the force sensor. The presence of the force sensor between the stage and the tool eliminates the need to include the dynamics of the stage in our model. Assuming a zero start position ($x(0) = 0$), the equilibrium point (x_h) can be calculated from Equation 2, where $f_{exerted} = f_a(0)$ and $x_{actual} = x(0)$. $f_a(0)$ is the initial applied force (within 12% of the target force) before the stage is allowed to move. The equilibrium point stays

stationary during the involuntary hand motion occurring within the first 20msec after the stage starts to move. Hence, \dot{x}_h is zero. Substituting the known variables in Equation 7 gives

$$(m_t + m_h)\ddot{x}(t) + b_h\dot{x}(t) + k_hx(t) = -f_a(t) + f_a(0) \quad (8)$$

The hand parameters (m_h , b_h , and k_h) are solved using the linear least-square method by rewriting Equation 8 as

$$\begin{bmatrix} \ddot{x}_i & \dot{x}_i & x_i \end{bmatrix} \begin{bmatrix} m_h \\ b_h \\ k_h \end{bmatrix} = -f_{ai} + f_a(0), \quad (9)$$

where $i = \{1 \dots 20\}$ refers to the time step at which the data was acquired. For each combination of user, grip force level, and target translational force, the data collected from three trials were concatenated and used to solve for the hand parameters as a single linear least-squares problem.

3.3 Hand Parameter Identification Results

Figure 5 shows the mass, damping, stiffness, and damping ratio of seven users (one user was an outlier) at different target translational forces at various grip force levels. The r^2 values were calculated to validate the results from the least-squares fit. The average of the r^2 of all trials across the seven users was 0.8. The effective hand masses found in our experiment fall between those of [8] and [12, 22]. This is likely because different grasps were used in each of these studies. Within the same grip force level, the effective mass, damping and stiffness coefficient estimates remain relatively constant across all amounts of translational force. The damping coefficients increase when the applied force is increased from 2N, however, they remain consistent between the force range of 4-8N. Comparing across the three grip force levels, the mass estimates are quite consistent. The damping coefficients are higher in general for the normal and hard grip cases than for the soft grip case. This is similar to what was found in [12]. However, the stiffness coefficients fall within the same range (between 500-1500 N/m) for all grip forces, unlike the increasing trend found in [9, 12]. Since the grip force was not measured, we do not know exactly how the users' actual grip force varied between the normal, hard, and soft cases. In our pushing task, grasping the tool "softly" is very unnatural, especially with high translational force. This could provide an explanation for the similar stiffness coefficients found between the various grip force levels. The damping ratios are relatively consistent among the users. On average for each user, the damping ratios with for the hard grip case are slightly higher than those in the normal and soft grip cases.

4 COMPARISON OF DYNAMIC VIRTUAL WALL METHODS

Given the hand dynamic parameters, we then implemented the Hand-Dynamic and Velocity-Based methods for selecting the location of a dynamic virtual wall to prevent penetration into a forbidden region. This experiment involved the same basic apparatus described in section 3.1. The stage motor was replaced with a non-backdrivable motor with a 128:1 gear ratio. In addition, a spring element was added between the stage and the tool to simulate joint compliance, as shown in Figure 6. Four highly elastic Nitinol strips were used to create the spring element. The tool position was obtained using a linear spring model, which was verified with a camera/vision system. The participants were the same eight users as in the hand model identification experiment.

The 1-DOF system was operated under admittance control, so the velocity of the stage was proportional to the translational force applied by the user when the tool is away from the forbidden region. To move the stage, the users pushed on the tool with a normal

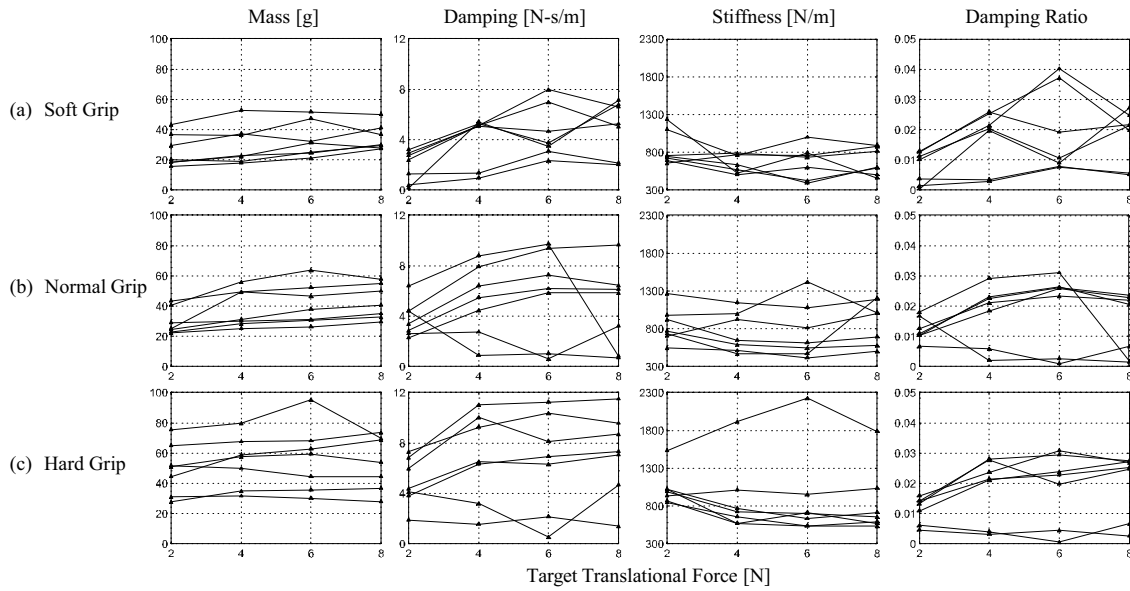


Figure 5: Measured hand parameters (Mass, Damping, Stiffness, and Damping ratio) for seven users with (a) Soft grip, (b) Normal grip, and (c) Hard grip. Each line represents the hand parameters of each user at four different target translational forces.

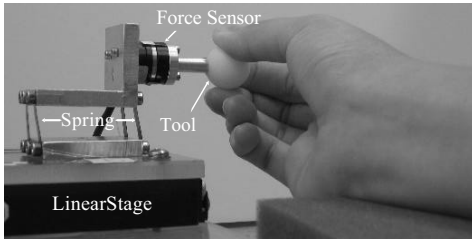


Figure 6: The 1-DOF dynamic virtual wall testbed with four Nitinol strips connecting the tool and the stage to simulate joint compliance.

gripping force. The users were asked to hold the tool with the same grip posture they used in the previous experiment. The stage was hidden from view, and the users had no visual feedback during the experiment.

In each trial, the users were asked to move the stage at a moderate speed in a single direction, and to switch directions when they encountered a virtual fixture. The forbidden region was randomly placed, and the users had no advance knowledge of its location. The users were instructed to not intentionally try to enter the forbidden region. Three methods were applied in random order to prevent the user from entering the forbidden region: Static Wall Method, Velocity-Based Method, and Hand-Dynamic Method. In the Static wall method, the virtual fixture position was kept fixed at the boundary of the forbidden region ($x_w = x_f$). The Velocity-Based and Hand-Dynamic Methods were implemented as described in Section 2. Each user performed a total of 15 trials, 5 with each method. The users practiced the task and were given rest time as needed. An admittance gain of $0.80 \frac{\text{mm}}{\text{Ns}}$ was used and kept constant throughout the experiment. All methods applied the same low-level PID-controller to achieve the desired stage velocity.

Through sample trials, we observed that users applied translational forces in the range of 5-10N while moving the stage. Based on the hand parameters found in the previous experiment (Figure 5b), we found the average upper and lower bounds of hand mass and stiffness coefficient within this force range. Investigation of Equation 5 shows that the maximum x_{r2} has an inverse relationship with hand mass. However, the relationship with stiffness is affected

by other parameters. Thus, in the Hand-Dynamic Method, we computed the maximum overshoot from the maximum mass and the worst case (either upper or lower bound) of the stiffness coefficient.

4.1 Results and Discussion

The penetration error, which is the distance between the maximum tool position and the forbidden region boundary, was measured and compared (Figure 7a). All users penetrated the forbidden region with the Static Wall Method. All users remained outside the forbidden region with the Velocity-Based and Hand-Dynamic Methods, which were not significantly different. However, comparing penetration errors directly may be misleading, since the users may approach the forbidden region with different amounts of translational force/velocity. To get a more accurate measure of how well the methods prevent the user from entering the forbidden region, the penetration error was divided by the force applied when the error occurred. This is shown as the error ratio in Figure 7b. A small negative error ratio is desirable since it indicates that the method is effective in preventing the tool from entering the forbidden region when a large force is applied. For both error metrics, the Hand-Dynamic Method offers a more conservative distance from the forbidden region as compared to the Velocity-Based Method. Since the Hand-Dynamic Method used the maximum/minimum bounds of the mass and stiffness coefficients found experimentally across all users, the overshoot calculated will be generally too conservative. A user-specific model may be needed for less conservative performance.

In this experiment, the tool was hidden from view to avoid the effect of the visual cues, which would be available in an actual application. Visual cues would certainly help prevent the user from moving the tool into a forbidden region. However, Boff and Lincoln reported that human visual response can take up to 150ms [6], which may be too long to prevent undesired involuntary hand motion. Furthermore, the visual information is often provided by an external sensor, whose data requires processing time and may not always be available due to occlusion. During the experiment, the users were asked to approach the forbidden region at a moderate speed. A separate test was done on a “malicious” user who moved at a high speed, intending to enter the forbidden region. The applied force recorded in this test was around 20N. The initial results

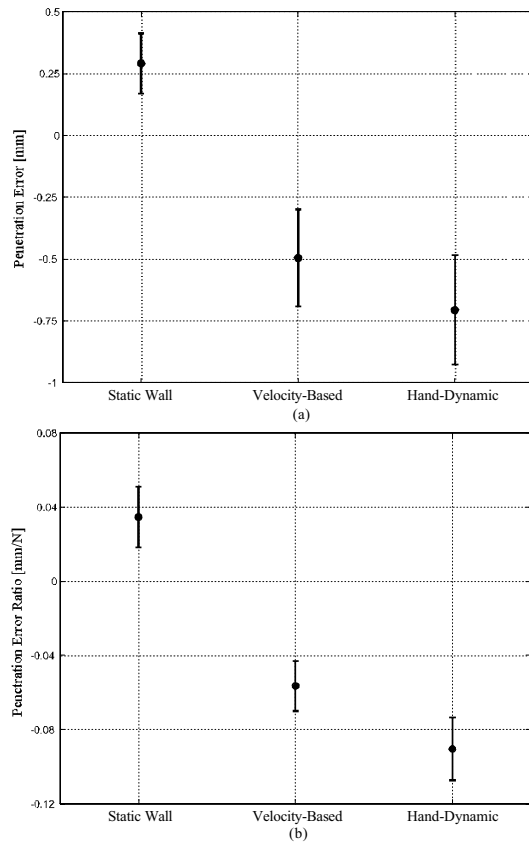


Figure 7: Comparison of the penetration errors (a) and the penetration error ratios (b) between the three virtual fixture methods. Positive values indicate penetration into the forbidden region.

from this single user showed that both of the dynamic virtual wall methods still prevented the tool from entering the forbidden region. The Hand-Dynamic Method was again slightly more conservative than the Velocity-Based Method.

The Velocity-Based Method is simple to implement, but has a major drawback. The maximum position determined by the method depends on the chosen time interval, Δt . One can easily imagine that the predictive method may not be fast enough to prevent tool penetration into the forbidden region if Δt is too small. 120msec was used as the time interval based on human reaction time, however, more analysis is needed to determine the optimal time interval to be used. Then, a more meaningful comparison of the two dynamic virtual wall methods can be made. In addition, both methods depend on the accuracy of the estimate of robot joint compliance. For the Hand-Dynamic Method, this dependency is shown in Equation 5. In the Velocity-Based Method, the overshoot inherently depends on the estimated joint compliance through the calculation of the tool velocity, v_t in Equation 1. Both methods can be applied to impedance-controlled devices, though the problem of link and joint compliance are not easily justified for such systems due to their design to be submissive to user force input. However, the underlying techniques for using system and hand dynamics to prevent the tool from entering into a forbidden region are still applicable. The predicted tool position can be treated as a proxy, which is commonly applied to create realistic user interaction in virtual and teleoperated environments. The predicted overshoot (d) can then be used to calculate the amount of force displayed back to user.

5 CONCLUSIONS AND FUTURE WORK

In this work, we examined the effect of human dynamics on the performance of a forbidden-region virtual fixture implemented on a 1-DOF admittance-controlled robot with joint compliance. The Velocity-Based and Hand-Dynamic Methods were proposed for defining a dynamic virtual fixture, whose distance from the boundary of the forbidden region varies depending on the instantaneous system dynamics. We conducted an experiment to determine the hand dynamic parameters (mass, damping and stiffness) for a combined active pushing/grasping task. The experiment shows that the effective mass, damping, and stiffness coefficients are quite constant within the same grip-force level for all amounts of applied translational force. The mass estimates and the damping coefficients are slightly higher in the hard and normal grip cases than the soft grip. The hand dynamic parameters found in the experiment were then used in the implementation of the Hand-Dynamic Method. The performance of the Velocity-Based and Hand-Dynamic Methods were verified experimentally on a 1-DOF testbed. The results show that the two methods effectively prevent the tool from entering into the forbidden region, in comparison to a static virtual fixture. The Hand-Dynamic Method, however, is more conservative than the Velocity-Based method.

Currently, the dynamic wall methods are implemented as an open-loop control on the virtual fixture position. When the condition in Equation 1 or 6 is met, the stage is stopped. This may leave the actual tool position at an undesirable distance away from the true forbidden region. A feedback loop can be added to move the position of the dynamic virtual wall closer to the true forbidden region based on the evolving system dynamics. Since the presence of virtual wall provides haptic cues to the user, the closed-loop implementation will create gradual haptic cues that help raise user awareness as the tool approaches the forbidden region. An adaptive control approach can be applied to adjust parameters according to the current state and the performance of the system. For example, we can adjust the hand dynamic parameters according to the amount of grip and applied force for a more user-specific implementation of the Hand-Dynamic Method.

In addition, the effective hand model considered here includes only the motion of the hand in extension from the wrist. We need to determine the hand dynamic parameters in other degrees of freedom for implementation of dynamic virtual walls in higher dimensions. The methods also need to be extended for guidance virtual fixtures, where the tool is maintained along a predefined path in space.

REFERENCES

- [1] J. J. Abbott, P. Marayong, and A. M. Okamura. Haptic virtual fixtures for robot-assisted manipulation. *International Symposium of Robotics Research*, 2005.
- [2] S. Allin, Y. Matsuoka, and R. Klatzky. Measuring just noticeable differences for haptic force feedback: Implications for rehabilitation. *Symposium on Haptic Interfaces for Virtual Environments and Teleoperator Systems*, pages 299–302, 2002.
- [3] Ryan A. Beasley and Robert D. Howe. Model-based error correction for flexible robotic surgical instruments. In *Proceedings of Robotics: Science and Systems*, Cambridge, USA, June 2005.
- [4] A. Bettini, S. Lang, A. Okamura, and G. Hager. Vision assisted control for manipulation using virtual fixtures: Experiments at macro and micro scales. *IEEE International Conference on Robotics and Automation*, pages 3354–3361, 2002.
- [5] E. Bizzi, N. Hogan, F. A. Mussa-Ivaldi, and S. Giszter. Does the nervous system use equilibrium-point control to guide single and multiple joint movements. *Journal of Behavioral and Brain Sciences*, 15:603–613, 1992.

- [6] K. R. Boff and J. E. Lincoln. *Engineering data compendium: Human perception and performance*, volume 3. Wright-Patterson Air Force Base, Ohio, 1988.
- [7] W. J. Book. Recursive lagrangian dynamics of flexible manipulator arms. *International Journal of Robotics Research*, pages 87–101, 1984.
- [8] A. Z. Hajian and R. D. Howe. Identification of the mechanical impedance at the human finger tip. *Journal of Biomechanical Engineering*, 119:109–114, 1997.
- [9] C. J. Hasser and M. R. Cutkosky. System identification of the human hand grasping a haptic knob. *Symposium on Haptic Interfaces for Virtual Environments and Teleoperator Systems*, pages 171–180, 2002.
- [10] H. Kazerooni and P. M. Bobgan. Human induced instability in powered hand controllers. *IEEE Transactions Robotics and Automation*, pages 755–759, 1992.
- [11] K. Kosuge, Y. Fujisawa, and T. Fukuda. Control of robot directly maneuvered by operator. *IEEE/RSJ International Conference on Intelligent Robots and Systems*, pages 49–54, 1993.
- [12] K. J. Kuchenbecker, J. G. Park, and G. Niemeyer. Characterizing the human wrist for improved haptic interaction. *International Mechanical Engineering Congress and Exposition*, 72(1):591–598, 2003.
- [13] M. Li. *Intelligent robotic surgical assistance for sinus surgery*. PhD thesis, Johns Hopkins University, 2005.
- [14] M. Li and R. H. Taylor. Spatial motion constraints in medical robot using virtual fixtures generated by anatomy. *IEEE International Conference on Robotics and Automation*, pages 1270–1275, 2004.
- [15] R. Marino and M. W. Spong. Nonlinear control techniques for flexible joint manipulators: A single link case study. *IEEE International Conference on Robotics and Automation*, 3:1030–1036, 1986.
- [16] T. E. Milner and D. W. Franklin. Two-dimensional endpoint stiffness of human fingers for flexor and extensor loads. *Proceedings of the International Mechanical Engineering Congress and Exposition, ASME*, 57(2):649–656, 1995.
- [17] C. A. Moore, M. A. Peshkin, and J. E. Colgate. Cobot implementation of virtual paths and 3-d virtual surfaces. *IEEE Transactions Robotics and Automation*, 19(2):347–351, 2003.
- [18] S. Payandeh and Z. Stanisic. On application of virtual fixtures as an aid for telemanipulation and training. *Symposium on Haptic Interfaces for Virtual Environments and Teleoperator Systems*, pages 18–23, 2002.
- [19] L. Rosenberg. Virtual fixtures: Perceptual tools for telerobotic manipulation. *Proceedings of IEEE Virtual Reality International Symposium*, pages 76–82, 1993.
- [20] R. Taylor, A. Barnes, R. Kumar, P. Gupta, Z. Wang, L. Whitcomb, P. Jensen, E. de Juan, D. Stoianovici, and L. Kavoussi. Steady-hand robotic system for microsurgical augmentation. *International Journal of Robotics Research*, 18(12):1201–1210, 1998.
- [21] T. Tsuji, K. Goto, M. Moritani, M. Kaneko, and P. Morasso. Spatial characteristics of human hand impedance in multi-joint arm movements. *IEEE/RSJ International Conference on Intelligent Robots and Systems*, 1:423–430, 1994.
- [22] C. R. Wagner and R. D. Howe. Mechanisms of performance enhancement with force feedback. *World Haptics*, pages 21–29, 2005.
- [23] D. Wang and M. Vidyasagar. Control of a class of manipulators with a single flexible link-part i: Feedback linearization. *ASME Journal of Dynamic Systems, Measurement, and Control*, 113:655–661, 1991.
- [24] J. N. Weiss and L. A. Bynoe. Injection of tissue plasminogen activator into a branch retinal vein in eyes with central retinal vein occlusion. *Ophthalmology*, 108(12):2249–2257, 2001.